ISSN 1068-3666, Journal of Friction and Wear, 2017, Vol. 38, No. 6, pp. 490–496. © Allerton Press, Inc., 2017.

Efficiency Analysis of a Cycloid Reducer Considering Tolerance[1]

Anh-Duc Pham[a] and Hyeong-Joon Ahn[b, *]

[a] *Department of Software Convergence, Graduate School, Soongsil University, Seoul, South Korea*

[b] *Department of Mechanical Engineering, Soongsil University, Seoul, South Korea*

**e-mail: ahj123@ssu.ac.kr*

Received June 10, 2017

Abstract—High precision reducers such as cycloid reducers have been used to meet the mechanical system requirements of industrial robots for advantages such as: high reduction ratio, large torque capability, and high efficiency. Although efficiency of reducers is one of important performances, there are few studies on efficiency of a cycloid reducer considering its tolerance. This paper presents efficiency analysis of a cycloid reducer with tolerance using the approximate force distribution of an ideal cycloid reducer. First, we present an FE analysis of a cycloid reducer with tolerances. Then, we approximate force distribution of the cycloid reducer with tolerance using an ideal cycloid reducer without any tolerance. The approximated force distribution of the cycloid reducer can be easily calculated using the theory of the ideal cycloid reducer. Finally, efficiency analysis of the cycloid reducer is performed using the approximate force distribution. Tolerance has great effect on efficiency on a cycloid reducer.

Keywords: efficiency analysis, cycloid reducer, tolerance

DOI: 10.3103/S1068366617060113

INTRODUCTION

During their developing history, most robots are now becoming smaller, faster, smarter and more flexible for high productivity manufacturing environment using enhanced technologies such as smart sensors, high compact components and advanced control. Because of their improvement and convenience, industrial robots are used in wide range of applications such as: packing, welding, testing or assembling in automatic manufacturing chain [1]. As expectation of International Federation of Robotics (IFR), the world industrial robot population can be reached to more than 2 million units in year of 2017 [2, 3].

Nowadays, efficiency of industrial robots plays an important role not only for productivity and profit but also for green manufacturing system. Preventing resources waste and improving energy efficiency is becoming a standard in design of next generation robots [1]. In particular, more and more environmental friendly products are released with efficiency robots.

High precision reducers like harmonic drive and cycloid reducer are widely used to satisfy demand of mechanical characteristic requirements such as high reduction ratio, high stiffness and load capacity, compact structure and high efficiency. There are three main performance measures of these reducers: hysteresis curve, rotational transmission error (RTE) and efficiency [2–11].

In the top of all, efficiency of the precision reducer is most important criteria both to reduce energy consumption and to increases productivity of industrial robots. Efficiency is determined by ratio between useful output and total input power. Although efficiency should become 100% in ideal condition, efficiency of the precision reducer cannot be raised up to certain number due to friction and tolerance.

Some previous studies on efficiency of high precision reducers were performed. In early, efficiencies of a cycloid reducer, a harmonic drive and a planetary gear reducer were compared by Botsiber in 1956 [11]. Efficiency of a reducer depends on many factors: applied torque, operated speed, lubrication, number of teeth in engagement, geometrical accuracy of components [5–9]. Moreover, several theoretical analyses of efficiency considering friction and lubrication factors were performed from 1983 to 2016 [5, 6, 9–11]. However, there are few studies on efficiency of a cycloid reducer considering tolerance although tolerances are inevitable for manufacturing errors and thermal expansion.

This paper presents an efficiency analysis of cycloid reducer with tolerance using approximate force distribution. First we present an FE analysis of a cycloid reducer with tolerance, which is hereafter called by "toleranced cycloid reducer". Then, the force distribution of the toleranced cycloid reducer is approxi-

[1] The article is published in the original.

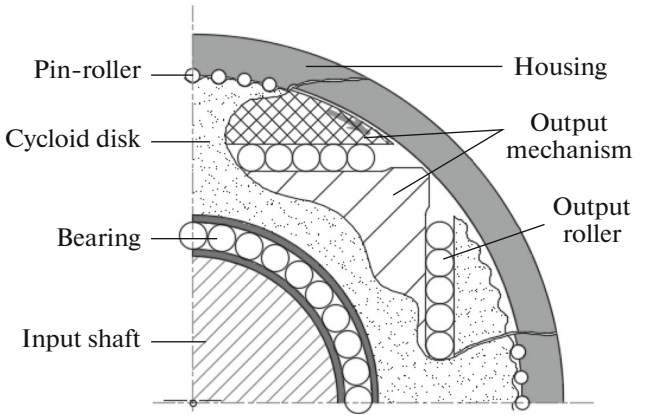

Fig. 1. A Cycloid reducer.

mated using that of an ideal cycloid reducer without any tolerance. Next, efficiency analysis of the toleranced cycloid reducer is performed using the approximate force distribution of the ideal cycloid reducer. Analysis results show that tolerance plays very importance role in efficiency of the cycloid reducer.

CYCLOID REDUCER CONSIDERING TOLERANCE

A one-stage cycloid reducer includes four main components: an input shaft, bearing, a cycloid disk and an output mechanism, as shown in Fig. 1. A pure rotation is actuated from the input shaft to the output mechanism by converting rotating motion to a wobble motion on the cycloid disk. In principle, the haft of pin-rollers on housing will be contacted with cycloid disk when input shaft is rotated [2, 3].

Figure 2a shows clearances between the cycloid disk and each pin roller with constant tolerance (5 and 10 μm) according to given parameters in Table 1.

Table 1. Specification of the cycloid reducer

Parameter	Value
Eccentricity e (mm)	0.35
Radius of housing R_h (mm)	32.5
Outer diameter of housing D_h (mm)	69
Radius of pin-roller R_r (mm)	0.8
Number of pin-roller Z_p	80
Number of output roller Z_o	40
Reduction ratio N	79
Radius of output roller R_o (mm)	1.5

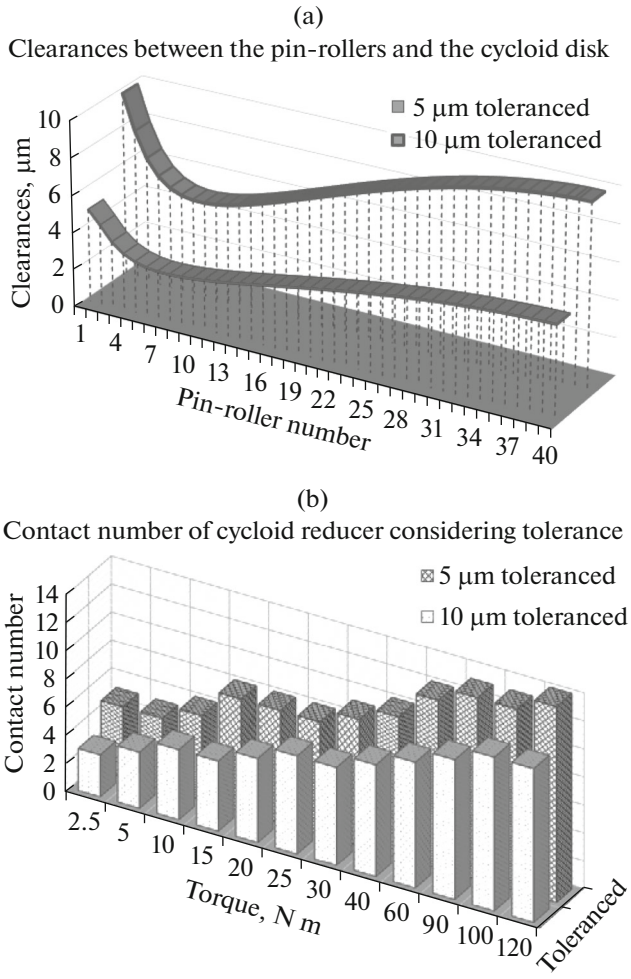

Fig. 2. Cycloid reducer with tolerance.

Clearance distributions change as the tolerance increases [2, 3, 12–14]. In order to determine the contact number of the cycloid reducer, FE analysis was performed using nonlinear springs with dead zone [3], as shown in Fig. 2b. The contact number is influenced by both of tolerance and applied torque. As the tolerance increases, contact number of the cycloid reducer decreases. On the other hand, the stronger torque results in the more contact number.

APPROXIMATE FORCE DISTRIBUTION OF THE TOLERANCED CYCLOID REDUCER

Principle

An ideal cycloid reducer without any tolerance is introduced to approximate force distribution of the toleranced cycloid reducer. This ideal cycloid reducer has the same contact number and a similar force distribution with toleranced cycloid reducer. Therefore, the number of cycloid lobes and pin-rollers of the ideal cycloid reducer is expressed with Eqs. (1–2). More-

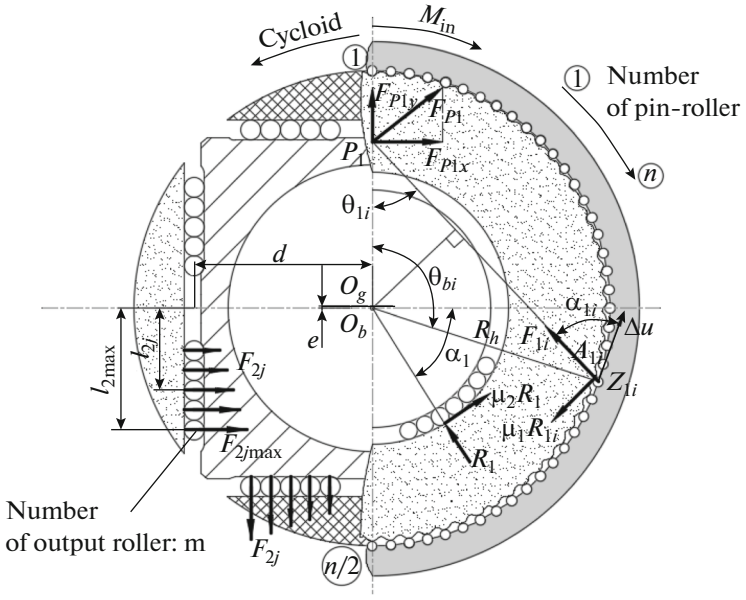

Fig. 3. Force diagram of one stage cycloid reducer with output mechanism.

over, radius of pin-rollers and housing are remained as same as the toleranced cycloid reducer in Table 1.

$$Z_g^e = 2n_c, \tag{1}$$

$$Z_P^e = 2n_c + 1 = Z_g^e + 1, \tag{2}$$

where, Z_g^e, Z_P^e: number of cycloid lobes and pin-rollers of the ideal cycloid reducer; n_c: contact number.

Theoretical Analysis of Contact Force Distribution

Free body diagram of the cycloid reducer under study is shown in Fig. 3. Here, O_g is center rotation of cycloid disk, O_b is origin-center of input shaft, P is pitch point of cycloid disk, and F_P is net force at pitch point P; F_{1i} is contact force between the ith pin-roller and cycloid disk. Assuming the input shaft rotates at a constant angular speed, the force and moment equilibrium equations can be written as Eq. (3). [2, 9, 12–14]

$$\begin{gathered}\sum F_x = 0; \quad \sum F_y = 0; \\ M_{\text{in}} = R_1(e\cos\alpha_1 + f_1(r + e\sin\alpha_1).\end{gathered} \tag{3}$$

We rewrite force and moment equilibrium in detail considering friction between the cycloid disk and pin-rollers, as shown in Eq. (4)–(6). Here, contact forces between the cycloid disk and the ith pin-rollers, the jth output roller are F_{1i}, F_{2j} ($i = 1–Z_p/2, j = 1–5$), respectively. f_1, f_2 are noted for frictions of bearing and cycloid disk. θ_{1i} is angle between contact force F_{1i} of ith pin roller and O_bP. Furthermore, α_1 is angle between the input bearing reaction force R_1 and horizontal direction. Under initial condition without any rotation of the sliding plate, $\beta_j = 90°$.

$$\begin{gathered}-\sum_{i=1}^{n/2} F_{1i}(\sin\theta_{1i} + f_1\cos\theta_{1i}) \\ + 4\sum_{j=1}^{m} F_{2i}\left(\sin\beta_j + \sin\left(\beta_j + \frac{\pi}{2}\right)\right) \\ - R_1(\cos\alpha_1 - f_2\sin\alpha_1) = 0,\end{gathered} \tag{4}$$

$$\begin{gathered}\sum_{i=1}^{n/2} F_{1i}(\cos\theta_{1i} - f_1\sin\theta_{1i}) \\ - 4\sum_{j=1}^{m} F_{2i}\left(\sin\beta_j + \cos\left(\beta_j + \frac{\pi}{2}\right)\right) \\ + R_1(\sin\alpha_1 + f_2\cos\alpha_1) = 0,\end{gathered} \tag{5}$$

$$M_{\text{out}} = 4\sum_{j=1}^{m} F_{2j}(d\cos\beta_j + l_{2j}\sin\beta_j). \tag{6}$$

Assuming the cycloid disk is fixed and moment M_{out} is applied to the housing, the moment makes pin roller rotate in very small angle around O_g. Furthermore, the pin-roller is rigid and deformation of the cycloid disk is ignored, center of each pin roller shifts in same circumferential displacement Δu. With analysis contact force between cycloid disk and pin-rollers in Fig. 3, we can find a component of displacement Δu along F_{1i}: $\Delta\varepsilon_i$ as shown in Eq. (7).

$$\Delta\varepsilon_i = \Delta u\cos\alpha_i = \Delta u\frac{l_{1i}}{R_h}. \tag{7}$$

The normal force F_{1i} is contact forces between the cycloid disk and pin rollers and P_1 is pitch point of the cycloid disk profile. Assuming contact force F_{1i} is proportional to $\Delta\varepsilon$ and contact stiffness is k_i, we can determine contact force with Eq. (8).

$$F_i \therefore k_i\Delta\varepsilon_i = k_i\Delta u\frac{l_{1i}}{R_h}. \quad (8)$$

Here l_{1i} is displacement from O_b to P_1Z_{1i}. Contact force F_{1i} in Eq. (8) can be rewritten by Eq. (9)

$$F_{1i} = F_{1\max}\frac{l_{1i}}{l_{1\max}} = F_{1\max}\frac{\overline{O_bP}\sin\theta_{1i}}{\overline{O_bP}} = F_{1\max}\sin\theta_{1i}. \quad (9)$$

Assuming the cycloid reducer is used in ideal working condition and friction force is neglected in comparing to value of contact force, substituting Eq. (9) into Eq. (4)–(5), we can rewrite Eq. (4)–(5) as Eq. (10):

$$\begin{gathered}-F_{1\max}\sum_{i=1}^{n/2}\sin^2\theta_{1i} \\ +4\sum_{j=1}^{m}F_{2j}\left(\sin\beta_j+\sin\left(\beta_j+\frac{\pi}{2}\right)\right)-R_1(\cos\alpha_1)=0, \\ F_{1\max}\sum_{i=1}^{n/2}\sin\theta_{1i}\cos\theta_{1i} \\ -4\sum_{j=1}^{m}F_{2j}\left(\cos\beta_j+\cos\left(\beta_j+\frac{\pi}{2}\right)\right)+R_1(\sin\alpha_1)=0.\end{gathered} \quad (10)$$

Approximate Force Distribution of the Ideal Cycloid Reducer

As shown in Eq. (9), force distribution of the ideal cycloid reducer depends on not only $F_{1\max}$ but also contact angle θ_1. $F_{i\max}$ is directly determined by moment output M_{out}. Whereas, contact angle in each pin θ_{1i} is totally dependent on geometrical parameters of the cycloid reducer as shown in Eqs. (11)–(13).

$$\sin\theta_1 = \sqrt{1-\cos\theta_1^2}, \quad (11)$$

$$\cos\theta_1 = \frac{-r_h^2+r_2^2+d_1^2}{2r_2d_1}, \quad (12)$$

$$\begin{gathered}d_1 = \sqrt{r_h^2+r_2^2-2r_2r_h\cos\theta_{b1}}, \\ \text{with:}\quad \theta_{b1} = i\frac{2\pi}{Z_p}.\end{gathered} \quad (13)$$

As seen from Eq. (13), there are three key geometrical parameters for force calculation of the ideal cycloid reducer: base circle radius of the pin-roller r_2, radius of housing r_h and angular position of pin-roller θ_{b1}. Angle of pin-roller θ_{b1} is related to position of pin-roller and determined by number of pin-roller.

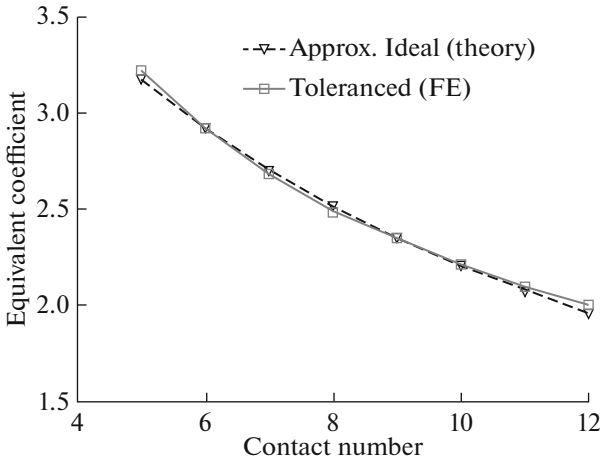

Fig. 4. Relationship between contact number and equivalent ideal profile of cycloid reducer.

Whereas, r_h is determined by size of the housing; r_2 is calculated by multiplying eccentricity e and number of cycloid lobes on cycloid disk Z_g.

Eccentricity and output torque are scaled using a coefficient C_e "torque coefficient", as shown in Eq. (14). The relationship between torque coefficient and contact number can be fitted with a polynomial of (Z_g^e/Z_g) as shown Eq. (15) and Fig. 4. Contact force of the toleranced cycloid reducer (FE analysis) and the ideal cycloid reducer are compared in Fig. 5. The ideal cycloid reducer approximates the toleranced cycloid reducer very well.

$$e^e = c_e e, \quad M_{\text{out}}^e = M_{\text{out}}/c_e, \quad (14)$$

$$\frac{1}{a\left(\dfrac{Z_g^e}{Z_g}\right)+b}\quad (a=1.1;\ \ b=0.176). \quad (15)$$

Bearing force and contact force of output rollers are compared between theoretical calculation and FE analyses in Figs. 6 and 7. Bearing forces of the toleranced and the ideal cycloid reducers are calculated using Eq. (10). In addition, contact force of output rollers F_{2j} is calculated with Eq. (6). The length arm l_{2j} of contact force F_{2j} of output roller is determined by assembling position (l_{2j} = 17 mm ~5 mm, j = 1~5).

EFFICIENCY OF CYCLOID CONSIDERING TOLERANCE BY USING EQUIVALENT IDEAL PROFILE OF CYCLOID REDUCER

Efficiency of a cycloid reducer is determined by ratio between useful output and input power. Friction and tolerance may cut off efficiency of the cycloid reducer. In that case, the useful output is calculated by

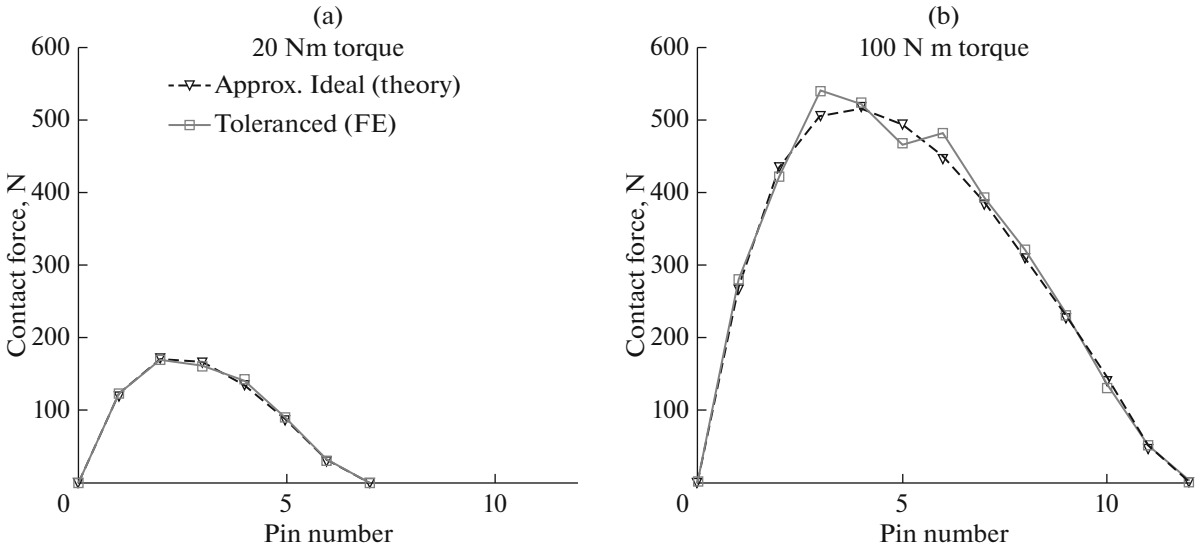

Fig. 5. Contact force distribution between the original and the equivalent ideal profile of cycloid reducer with 10 μm tolerance.

subtracting power loss (P_{loss}) from input power (P), as shown in Eq. (16)

$$\eta = \frac{P - P_{loss}}{P}. \quad (16)$$

Based on structure of the cycloid reducer as shown in Fig. 1, the power loss consists of three main parts: bearing loss ($L_{bearing}$), power loss at contacts between cycloid disk and pin-roller ($L_{cycloid}$), and output mechanism loss (L_{output}), as shown in Eq. (17).

$$P_{loss} = L_{bearing} + L_{cycloid} + L_{output}. \quad (17)$$

Equations for calculating losses at each component are summarized in Table 2 [11, 15]. Although there are many ways to calculate, bearing loss can be divided into load-independent and load-dependent losses, as in Eq. (18)–(20) [11, 15]. Here, d_M, υ are defined for mean bearing diameter of bearing and kinematic viscosity of lubricant, respectively; $\upsilon = 15$ (mm^2/s) with viscosity ratio $\kappa = 1$, operating temperature 40°C and operating speed ≥ 2400 (rpm) for bearing model 6202 [15]. In addition, the cycloid loss is defined by sum of power losses at each contact loss between cycloid disk and pin-roller as in Eq. (21); the contact loss between cycloid and pin-roller is calculated by multiplication of friction force and both sliding and rolling velocities at each pin-roller. Based on kinematics analysis of the cycloid reducer, rolling and sliding velocities of pin-rollers are introduced in Eq. (22)–(23) [11]. Finally, output mechanism loss is based on loss in contact between output rollers and output parts as shown in Eq. (24). Relationship between input and output angular velocities is illustrated in Eq. (25) [2].

A diagram for efficiency analysis of the toleranced cycloid reducer is shown as in Fig. 8. First, contact number and contact position are predicted based on

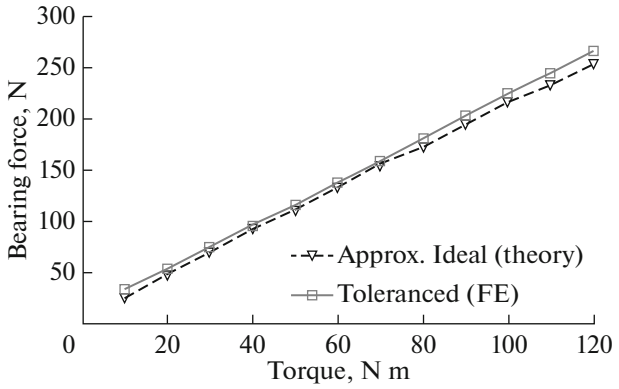

Fig. 6. Bearing force by various output torque with 5 μm tolerance.

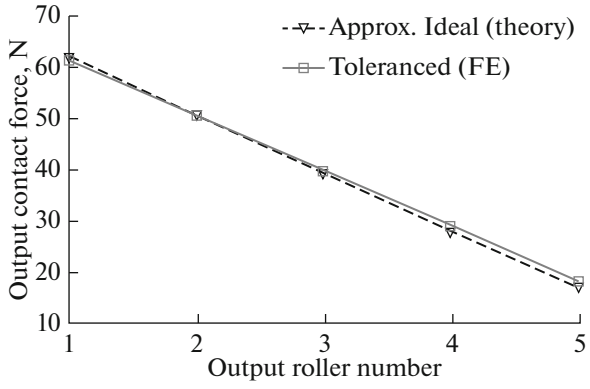

Fig. 7. Contact force of output with 10 Nm torque.

Table 2. Loss of the cycloid reducer calculation

Part	Equation
Bearing	$L_{\text{bearing}} = T_{\text{bearing}} \frac{\omega_{\text{in}}}{9550} = (T_o + T_1) \frac{\omega_{\text{in}}}{9550}.$ (18) Fictional torques as a function of speed: $T_0 = f_0 (\nu \omega_{\text{in}})^{2/3} d_M^3 \times 10^{-7}.$ (19) Frictional torques as a function of torque: $T_1 = f_1 R_1 d_M$ (20) *f_0, f_1 are chosen following characteristics of bearing model 6202 ($f_0 = 1.3$ and $f_1 = 0.0013$)
Cycloid	$L_{\text{cycloid}} = f_2 \sum_{i=1}^{n} V_i F_{1i} \Sigma = f_2 \sum_{i=1}^{n} (V_{\text{rolling\_}i} + V_{\text{Sliding\_}i}) F_{1i},$ (21) $V_{\text{rolling\_}i} = \omega_{\text{in}} \cos(\pi - \theta_{1i}) \left(-e + 2 \frac{r_2 R_r}{P_1 A_{1i}} \right),$ (22) $V_{\text{Siding\_}i} = -\omega_{\text{in}} e \cos(\pi - \theta_{1i}) + \omega_{\text{out}} P_1 A_{1i} \cos(\pi - \theta_{bli} - \theta_{1i})$ (23)
Output mechanism	$L_{\text{output}} = f_3 \sum_{j=1}^{m} V_j F_{2j} = f_3 \sum_{j=1}^{m} \omega_{\text{out}} l_{2j} F_{2j}$ (24) with $\omega_{\text{out}} = \frac{\omega_{\text{in}}}{N}$ (25) $f_2 = f_3 = 0.015.$

tolerance and applied torque. Then, approximate contact force distribution is calculated using the ideal cycloid reducer and velocity at each contact point between cycloid disk and pin-roller is determined based on Eq. (22)–(23). In the end, efficiency of cycloid reducer is calculated based on equations in Table 2.

By varying applied torques and input speeds, efficiency of the cycloid reducer is calculated and shown in Figs. 9 and 10. Tolerance has great effect on efficiency of the cycloid reducer. In case of the cycloid reducer without any tolerance, its efficiency doesn't change much according to variations of torque and operating speed. On the other hand, efficiency of the toleranced cycloid reducer decreases significantly as torque decreases.

Influence of tolerance on efficiency of the cycloid reducer is shown in Fig. 9. In the range of 30% rated torque, efficiency of the toleranced cycloid is smaller by 12–17% than that of cycloid reducer without any tolerance. As applied torque increases, the efficiency of the toleranced cycloid reducer goes substantially up to that of the cycloid reducer without tolerance. At its rated torque, the efficiency of the toleranced cycloid reducer is only 4% lower than that of the cycloid reducer without tolerance. The main reason is the change of contact number according to increasing applied torque in the toleranced cycloid reducer.

The higher speed cycloid results in the lower efficiency, as shown in Fig. 10. However, in case of high applied torque, the operating speed has small effect on efficiency of the cycloid reducer. Whereas, the operating speed has a significantly influence on efficiency of the toleranced cycloid reducer under torque lower than 30% of its torque.

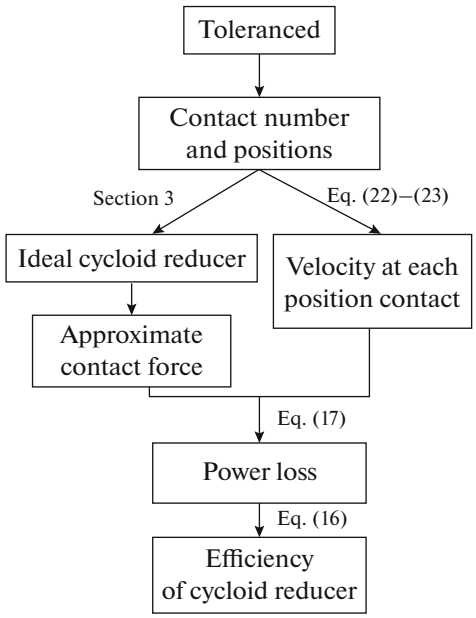

Fig. 8. Analysis diagram of efficiency cycloid reducer using approximate force distribution.

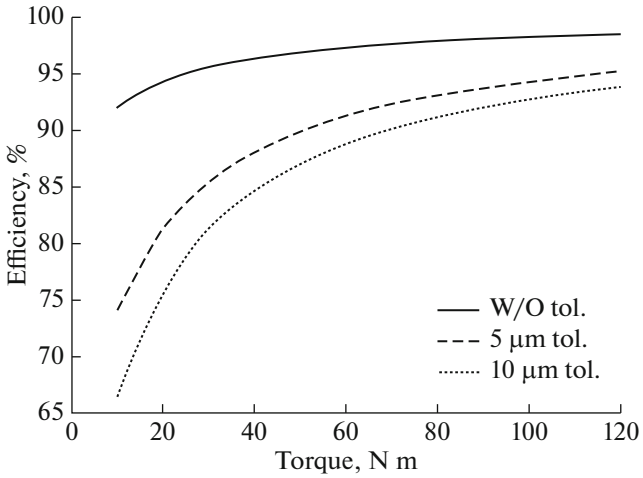

Fig. 9. Efficiency of the toleranced cycloid reducer under various applied torques.

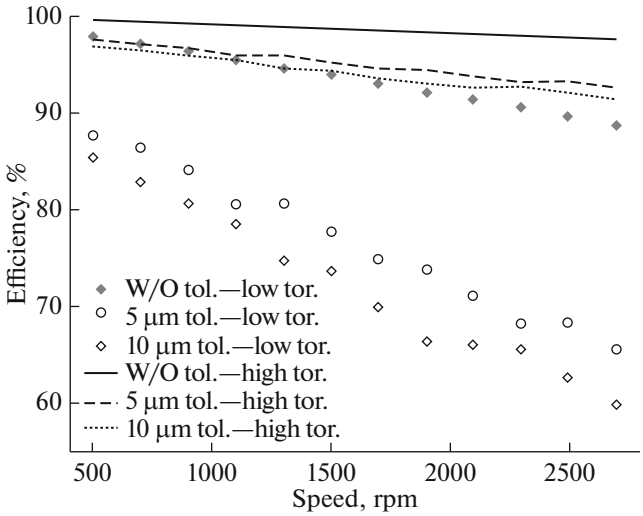

Fig. 10. Efficiency of the toleranced cycloid reducer with various operating speeds.

CONCLUSIONS

This paper presents efficiency analysis of a cycloid reducer with tolerance using the approximate force distribution of an ideal cycloid reducer. The force distribution of the toleranced cycloid reducer by FE analysis is approximated using that of an ideal cycloid reducer without any tolerance. Efficiency analysis of the toleranced cycloid reducer is performed using the equivalent force distribution based on the approximate force distribution of the ideal cycloid reducer. Tolerance had a great effect on efficiency of cycloid reducer.

From analysis results, it is easily seen that both of operating speed and torque influence on efficiency of the toleranced cycloid reducer. In model of cycloid reducer without any tolerance, its efficiency doesn't change much by varying torque and operating speed. However, efficiency of the toleranced cycloid reducer is significantly reduced as decreasing torque or increasing speed with maximum 25% in loss power.

REFERENCES

1. Brogardh, T., Present and future robot control development—an industrial perspective, *Ann. Rev. Control*, 2007, vol. 31. pp. 69–79.
2. Tran, T.L., Pham, A.D. and Ahn, H.J., Lost motion analysis of one stage cycloid reducers considering tolerances, *J. Precis. Eng. Manuf.*, 2016, vol. 17, no. 8, pp. 1009–1016.
3. Pham, A.D., Tran, T.L., and Ahn, H.J., Hysteresis curve analysis of a cycloid reducer using non-linear spring with a dead zone, *J. Precis. Eng. Manuf.*, 2017, vol. 18, no. 3, pp. 375–380.
4. Kircanski, N.M. and Goldenberg, A.A., An experimental study of nonlinear stiffness, hysteresis, and friction effects in robot joints with harmonic drives and torque sensors, *Int. J. Rob. Res.*, 1997, vol. 16, no. 2, pp. 214–239.
5. Csoban, A. and Kozma, M., Influence of the oil churning, the bearing and the tooth friction losses on the Efficiency of planetary gears, *J. Mech. Eng.*, 2010, vol. 56, no. 4, pp. 231–238.
6. Bao, J. and He, W., Parametric design and efficiency analysis of the output-pin-wheel cycloid transmission, *Int. J. Control Autom.*, 2015, vol. 8, no. 8, pp. 349–362.
7. Hohn, B.R., Stahl, K. and Gwinner, P, "Improved efficiency for high-ratio planetary gear transmissions, *Proc. Int. Conf. on Gears*, Munich, 2013.
8. Mihailidis, A., Nerantzis, I. and Athanasopoulos, E., Cycloid and Wolfrom reducers for applications requiring high accuracy, high ratio and high torque rating, *Proc. Int. Conf. on Gears*, Munich, 2013, pp. 697–708.
9. Malhotra, S.K. and Parameswanran, M.A., Analysis of a cycloid reducer, *Mech. Mach. Theor.*, 1983, vol. 18, no. 6, pp. 491–499.
10. Schafer, I., Bourlier, I., Hantschack, F., Roberts, E.W., Lewis, SD., Forster, D.J. and John, C., Space lubrication and performance of harmonic drive gears, *Proc. 11th ESMATS: European Space Mechanisms and Tribology Symp.*, Lucerne, 2005, pp. 65–72.
11. Mihailidis, A., Athanasopoulos, E. and Agouridas, K., EHL film thickness and load dependent power loss of cycloid reducers, *Mech. Mach. Theor.*, 12016, vol. 230, nos. 7–8, pp. 1303–1317.
12. Blanche, J.G. and Yang, D.C.H., Cycloid drives with machining tolerances, *J. Mech., Transm., Autom. Des.*, 1989, vol. 111, pp. 337–344.
13. Yang, D.C.H. and Blanche, J.G., Design and application guidelines for cycloid drives with machining tolerances, *Mech. Mach. Theor.*, 1990, vol. 25, no. 5, pp. 487–501.
14. Ren, Z.Y, Mao, S.M., Guo, W.C, and Guo, Z., Tooth modification and dynamic performance of the cycloidal drive, *Mech. Syst. Signal Process.*, 2017, vol. 85, pp. 857–866.
15. *Lubricant of Rolling Bearing*, Herzogenaurach: Schaeffler Technologies, 2013.